Distinct pairing symmetries in $Nd_{1.85}Ce_{0.15}CuO_{4-y}$ and $La_{1.89}Sr_{0.11}CuO_4$ single crystals: Evidence from comparative tunneling measurements

L. Shan,[1,*] Y. Huang,[1] H. Gao,[1] Y. Wang,[1] S. L. Li,[2] P. C. Dai,[2,3] F. Zhou,[1] J. W. Xiong,[1] W. X. Ti,[1] and H. H. Wen[1,†]
[1]*National Laboratory for Superconductivity, Institute of Physics, Chinese Academy of Sciences, P.O. Box 603, Beijing 100080, China*
[2]*Department of Physics and Astronomy, The University of Tennessee, Knoxville, Tennessee 37996-1200, USA*
[3]*Center for Neutron Scattering, Oak Ridge National Laboratory, Oak Ridge, Tennessee 37831-6393, USA*
(Received 14 March 2005; revised manuscript received 11 July 2005; published 7 October 2005)

We used point-contact tunneling spectroscopy to study the superconducting pairing symmetry of electron-doped $Nd_{1.85}Ce_{0.15}CuO_{4-y}$ (NCCO) and hole-doped $La_{1.89}Sr_{0.11}CuO_4$ (LSCO). Nearly identical spectra without zero bias conductance peak (ZBCP) were obtained on the (110) and (100) oriented surfaces (the so-called nodal and anti-nodal directions) of NCCO. In contrast, LSCO showed a remarkable ZBCP in the nodal direction as expected from a *d*-wave superconductor. Detailed analysis reveals an *s*-wave component in the pairing symmetry of the NCCO sample with $\Delta/k_BT_c=1.66$, a value remarkably close to that of a weakly coupled Bardeen-Cooper-Schriffer (BCS) superconductor. We argue that this *s*-wave component is formed at the Fermi surface pockets centered at $(\pm\pi,0)$ and $(0,\pm\pi)$ although a *d*-wave component may also exist.

DOI: 10.1103/PhysRevB.72.144506 PACS number(s): 74.50.+r, 74.72.Jt, 74.45.+c

I. INTRODUCTION

For hole-doped cuprate superconductors, there is a well-known electronic phase diagram characterized by a dome-like superconducting region when p is above a certain threshold.[1] It was found that[2] instead of doping holes into the Cu-O plane, one can also achieve superconductivity by doping electrons into the Cu-O plane in systems like $Ln_{2-x}Ce_xCuO_4$ with Ln=Nd, Pr, La, etc. One thus naturally questions whether the superconducting mechanism is the same between the hole- and electron-doped cuprates. Among many superconducting properties, the symmetry of the order parameter is an important one. While the symmetry of the superconducting order parameter is believed to be *d*-wave for the hole-doped region,[3] the situation for electron-doped materials is highly controversial. For example, angle-resolved photoemission spectroscopy (ARPES),[4] specific heat,[5] phase-sensitive scanning SQUID,[6] bi-crystal grain-boundary Josephson junction,[7] and some penetration depth measurements[8,9] indicate a *d*-wave symmetry. In addition, Raman scattering[10] and recent ARPES[11] experiments show a nonmonotonic *d*-wave order parameter. However, this has been contrasted by tunneling[12,13] and some other specific heat[14] and penetration depth measurements.[15–17] In particular, there may be a crossover from *d*-wave to *s*-wave symmetries by changing the doped electron concentration[18,19] or decreasing the temperature.[20] Although such a crossover may explain the conflicting experimental results on the pairing symmetry in the electron-doped cuprates, the characteristics of such possible *s*-wave pairing symmetry has yet to be established.

In this paper, we report directional tunneling measurements on single crystals of optimally electron-doped cuprate $Nd_{1.85}Ce_{0.15}CuO_{4-y}$ (NCCO). By injecting current along either the Cu—Cu bond (110) or Cu—O bond (100) direction, we obtain nearly identical tunneling spectra indicating an *s*-wave component of the pairing symmetry in this material. For comparison, similar measurements were carried out on underdoped *p*-type single crystals of $La_{1.89}Sr_{0.11}CuO_4$ (LSCO), and we observed clear zero bias conductance peaks (ZBCP) in tunneling spectra along the (110) direction as expected from the $d_{x^2-y^2}$-wave symmetry. Our results thus indicate that the optimally doped NCCO has at least an unavoidable *s*-wave component, which is in contrast with the case in hole-doped LSCO where a pure *d*-wave has been established.

II. EXPERIMENTAL DETAILS

We grew the NCCO and LSCO single crystals using the traveling-solvent floating-zone technique.[21,22] As shown in Fig. 1, the resistive curve measured on the NCCO sample indicates a zero-resistance temperature at 25.1 K, AC susceptibility shows the onset of bulk superconductivity at T_c

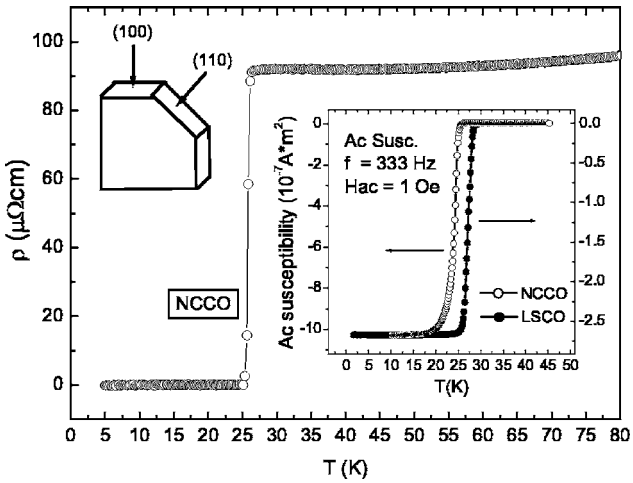

FIG. 1. The temperature dependence of resistivity for the sample NCCO. The insets show the AC susceptibility of NCCO and LSCO. The schematic diagram of the point contact configuration are presented in the upper left of the main panel.

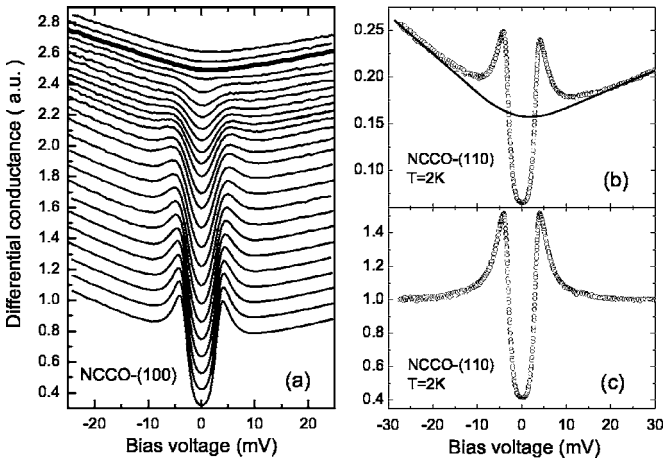

FIG. 2. Raw data of the directional spectral measurements. (a) The temperature dependent tunneling spectra measured along (100) direction. The curves have been shifted for clarity. The temperature increases from the bottom up with the steps of 1 K (from 2 to 22 K) and 2 K (from 22 to 30 K). The thick solid line denotes the data at 26 K which is around T_c. (b) An illustration of constructing normal conductance background according to the functional form of the spectra above T_c. (c) Normalized spectrum for (110) direction at $T=2$ K.

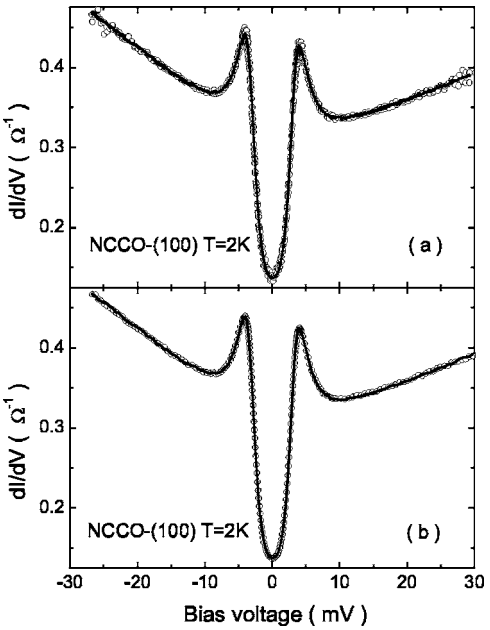

FIG. 3. Comparison between the $\sigma \sim V$ curves: (a) obtained from lock-in technique (solid line) and DC $I \sim V$ measurements (open circles); (b) measured with positive (solid line) and negative (open circles) bias scanning.

≈ 25.6 K. The LSCO sample has a $T_c \approx 28$ K characterized by AC susceptibility measurement. The single crystals used in the tunneling measurements were cut into rectangular flakes of size $2.5 \times 2.5 \times 1$ mm^3 for NCCO and $1.5 \times 1.5 \times 0.8$ mm^3 for LSCO with the long axis along a (100) or b (010) and short axis along c (001), one corner of the crystal was then cut off to expose the (110)-oriented crystal planes. The directional point-contact tunneling measurements were carried out by pointing a Pt/Ir alloy tip or Au tip toward the specified directions as shown in the left inset of Fig. 1. The tip's preparation and the equipment details are described in Ref. 23. In order to reduce quasiparticle scattering in the barrier layer and obtain high quality data, the nonaqueous chemical etch was used to attenuate the insulating layer on the sample surface immediately before mounting the sample on the point contact device. Since it takes about 20 to 40 minutes to insert the sample mounted device into the Helium gas environment in the dewar, the sample surfaces were exposed to air during this period. For chemical etching, we used 10% HCl in absolute ethanol for several seconds to several tens of seconds for NCCO and 1% Br_2 in absolute ethanol for several minutes to ten minutes in the case of LSCO. Typical four-terminal and lock-in techniques were used to measure the $I \sim V$ curves and the differential resistance dV/dI vs V of the point contacts.

III. RESULTS AND DISCUSSION

A. Tunneling spectra of $Nd_{1.85}Ce_{0.15}CuO_{4-y}$ (NCCO)

Figure 2 shows the raw data of the conductance (σ) of Au/NCCO point contact for various temperatures from 2 to 30 K. In order to show the electronic stability of the experiments, we simultaneously present in Fig. 3(a) the $\sigma \sim V$ curves obtained from the lock-in technique and DC $I \sim V$ measurement, respectively. It is obvious that these two curves merge into each other although the latter one has a higher noise. We also compared the $\sigma \sim V$ curves recorded by both positively and negatively scanning the bias voltage. As shown in Fig. 3(b), the complete overlap of the data with different scanning directions indicates the good thermal stability during measurements.

It is well known that the high T_c superconducting cuprate compounds react readily with atmospheric H_2O and CO_2 to form insulating hydroxides and carbonates on the surface and at grain boundaries.[24] While such a poor conductive layer may be a natural barrier needed in tunneling experiments, they may introduce a large scattering factor (just like the situation of fabricated planar junction) and thus result in less sharpening spectra than those measured by the vacuum barrier based scanning tunneling microscopy (STM).[25] In order to reduce the scattering factor and obtain sharp spectra, we used nonaqueous chemical etch to treat the sample surfaces.[24,26] In Fig. 4, we present the measured spectra on the surfaces as cut, after the first etch and after the second etch, all the spectra have been normalized for comparison. The detailed experimental conditions are listed in Table I. The experimental results indicate that the chemical etch can effectively reduce the thickness of the barrier layer on the surface of the NCCO single crystal and hence decrease the scattering factor.

We also studied the dependence of the measured spectrum on the junction resistance which can be controlled by adjusting the tip-to-sample distance with a differential screw. Figure 5 shows the spectra measured at a fixed position on the sample surface as a function of junction resistances, in these measurements the sample surfaces had been chemically

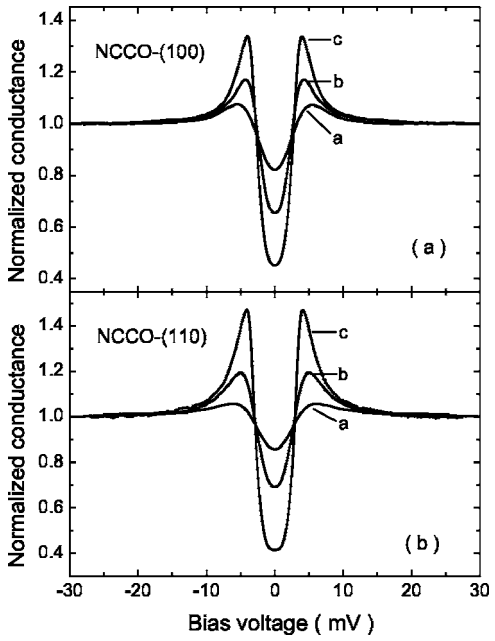

FIG. 4. The normalized $\sigma \sim V$ curves obtained by different surface treatments and using different tips. Note that the spectra measured on the post-etched surfaces are much sharper than those of pre-etched ones, accompanied by a remarkable decrease in the junction resistance from several hundreds of ohms to below 10 Ω, as shown in Table I.

etched. When the junction resistance decreases from several tens of ohms to several ohms, the spectral shape becomes sharper [refer to Fig. 8(a)]. For small resistance, the spectral shape hardly changes with the resistive values and no Andreev reflection-like spectrum occurs[27] (Fig. 5). This indicates that although the surface contaminant phase has been reduced, it still exists as a solid barrier layer due to the exposure to air. After the metal tip reaches the sample surface, the barrier layer is abraded at first and its thickness decreases with the increasing pressure. Consequently, the measured spectrum becomes sharper due to the weakening of the inelastic scattering of the injecting quasiparticles near the normal-metal/superconductor (N/S) micro-constriction. Further pressure of the tip on the sample surface may simply flatten the point, giving a larger contact area over the same minimal thickness of a tenacious barrier layer which cannot be entirely flaked off.[28] In this case, the junction resistance

TABLE I. List of the experimental conditions for the different spectra presented in Fig. 4.

Label	Chemical etch	Tip	$R_{20\,\mathrm{mV}}$ (Ω)
(110)-a	None (As cut)	Pt/Ir Alloy	197.0
(110)-b	By 10% HCl (20s)	Pt/Ir Alloy	75.7
(110)-c	By 10% HCl (60s)	Au	5.3
(100)-a	None (As cut)	Pt/Ir Alloy	170.0
(100)-b	By 10% HCl (20s)	Pt/Ir Alloy	19.9
(100)-c	By 10% HCl (60s)	Au	2.9

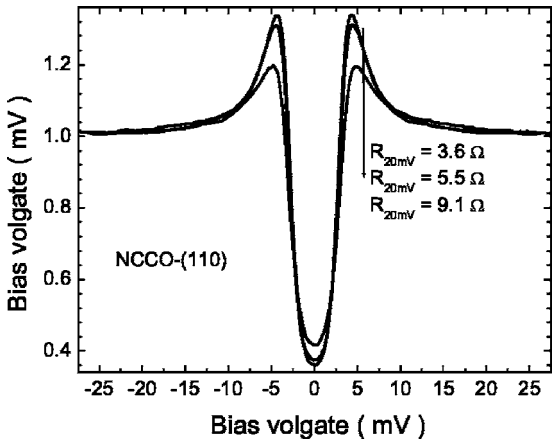

FIG. 5. The normalized $\sigma \sim V$ curves measured at a fixed position on the sample surface with various junction resistance.

becomes still smaller while with no obvious change on the measured spectrum until the junction is damaged eventually. Therefore, the non-zero bias conductance should be ascribed to the stronger scattering effect on injecting quasiparticles and lower height of the surface barrier than that of the vacuum barrier. Nonetheless, such surface contaminants resulting from air exposure form at orders of magnitude slower on NCCO than on many hole-doped cuprates which results from the absence of reactive alkaline earth elements in NCCO.[26] This is also the reason why the measured spectra of LSCO are poorer than that of NCCO using the same method, as shown in Sec. III C in this paper. In the following, we will focus our attention on the spectra with the resistance from 1 to 15 Ω, namely, in the regime with good spectral stability and weaker scattering effect.

In MaglabExa-12, the magnetic field can be applied along the tip's direction, namely, parallel to the *ab* plane. The field dependence of the tunneling spectra were measured at various temperatures from 4 to 16 K. The changing tendency of the spectral shape with increasing field is identical at all measured temperatures. The typical results of 4 and 10 K in Fig. 6 suggest that the field induced smearing of the spectrum is very slight, which is consistent with the much higher H_{c2} than 7 T for $H \| ab$-plane.

To sum up the main characteristics of the measured spectra, we note that all the spectra are near the tunneling limit with two clear coherence peaks at symmetric positions of the bias voltage (much sharper than that of the previous works studied by both STM[13,29] and point contact)[30] with no Andreev reflection-like spectrum. Second, the spectral shape is nearly identical for the (110) and (100) directions. Third, there was no evidence for zero-bias conductance peak (ZBCP) expected in the (110) (or the so-called nodal direction) of the *d*-wave superconductors.[31–33] Here we emphasize that the results are independent of the positions on the sample surface.

B. *S*-wave Blonder-Tinkham-Klapwijk (BTK) theory

As discussed above, if the superconducting NCCO has *d*-wave pairing symmetry, a ZBCP should be observed in the

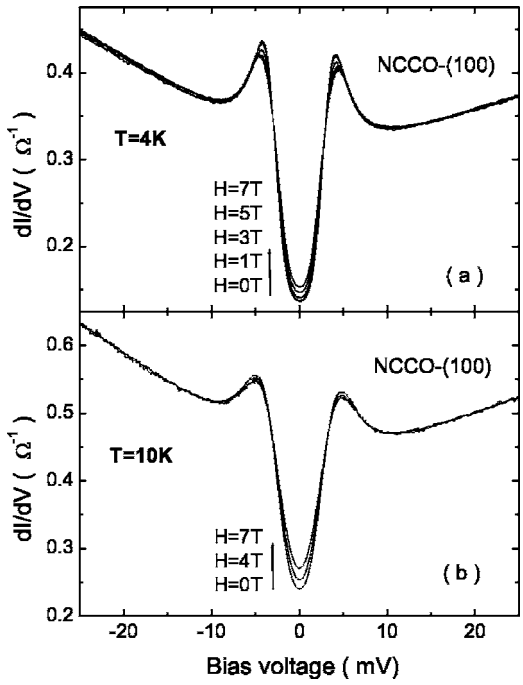

FIG. 6. The magnetic field dependence of the tunneling spectra measured at (a) 4 K and (b) 10 K. The very small modification of the spectral shape in field up to 7 T indicates that we indeed measured the bulk superconductivity of NCCO.

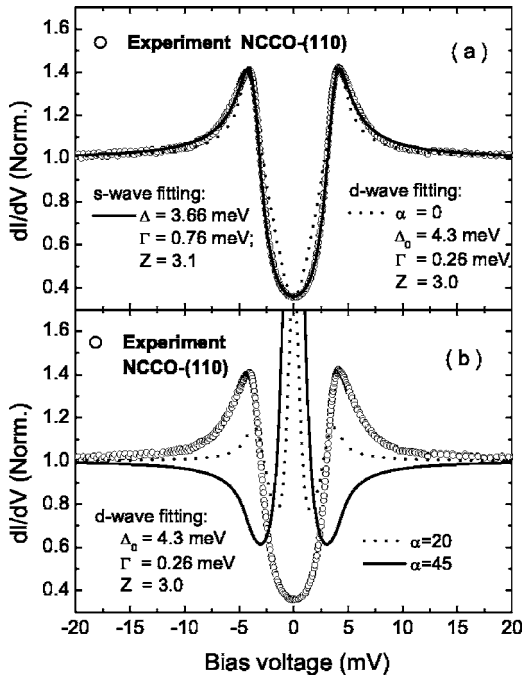

FIG. 7. The comparison of fitting the normalized conductance measured along (110)-direction at 2 K to the *s*-wave model and $d_{x^2-y^2}$-wave model. For, *d*-wave fitting, α denotes the angle between the normal direction of the sample surface and the crystallographic axis *a*. Note that the *s*-wave fitting is much better than the *d*-wave fitting.

(110)-oriented tunneling spectrum. In other words, our experimental results suggest that the optimally doped NCCO has a *s*-wave symmetry. In order to explain this viewpoint, we present in Fig. 7 the best fitting of the (110)-oriented tunneling spectrum with the formulas corresponding to *s*- and *d*-wave models, respectively. For the simulations, the extended BTK model[27,32] was accepted by selecting a constant gap value for *s*-wave symmetry and the anisotropic gap of $\Delta(\theta)=\Delta_0\cos(2\theta)$ for $d_{x^2-y^2}$ symmetry, where θ is the polar angle measured from the crystallographic axis *a*. In this model, two parameters are introduced to describe the necessary physical quantities, i.e., the effective potential barrier (Z) and the superconducting energy gap (Δ). As an extension, the quasiparticle energy E is replaced by $E-i\Gamma$, where Γ is the broadening parameter characterizing the finite lifetime of the quasiparticles due to inelastic scattering near the N/S micro-constriction.[34,35] In a real N-I-S junction configuration, the total tunneling conductance spectrum includes the integration over the solid angle. In the case of two dimensions, it reduces to the integration over the injection angle from $-\pi/2$ to $\pi/2$, as done in this work. Figure 7(b) clearly shows that the *d*-wave theoretical simulation along the (110) direction deviates from the experimental data. When the normal direction of the sample surface departs a small angle from the crystallographic axis *a*, a ZBCP will appear, accompanied by the remarkable depression of the coherence peaks. As shown in Fig. 7(a), even the *d*-wave simulation absolutely along (100) direction cannot fit the experimental data in the range below superconducting gap. However, the calculated curves in terms of the *s*-wave theory are in good agreement with the experimental results in both (100) and (110) directions.

It should be pointed out that the values of Z and Γ are related to the selected form of the background (such as the slope coefficient of the high bias straight-line segments) to a certain extent, which may be the main artificial uncertainty in the data analysis. So we did not focus our attention on the absolute values of these parameters or the quantitative comparison between the different spots. However, it is also found that the energy gap Δ is insensitive to the selection of different backgrounds in the fitting process. Moreover, when we chose a general procedure to construct the background for all spectra measured on a fixed spot on the sample surface, the variation of the fitting parameters of Z and Γ should be physically meaningful. As an example, we present in Fig. 8(a) the normalized spectra measured at a fixed spot with different junction resistance, which have been theoretically fitted to the *s*-wave BTK model and the fitting parameters are shown in Fig. 8(b). It is noted that the derived energy gap is nearly constant for all spectra, while the barrier height Z and broadening parameter Γ continuously decrease with the decreasing junction resistance. This is physically reasonable and in good agreement with the foregoing discussions, namely, the abrasion of the contaminant layer will depress the barrier height accompanied by the weakening of the quasiparticle scattering near the N/S micro-constriction.

The good spatial repeatability of the tunneling spectra allowed further investigations of their temperature dependence. The spectral shape changed continuously until above 24 K ($T_c \sim 26$ K), thus suggesting that the tunneling spectra reflect the bulk superconductivity of the NCCO sample [Fig. 2(a)]. The temperature-dependent normalized spectra for

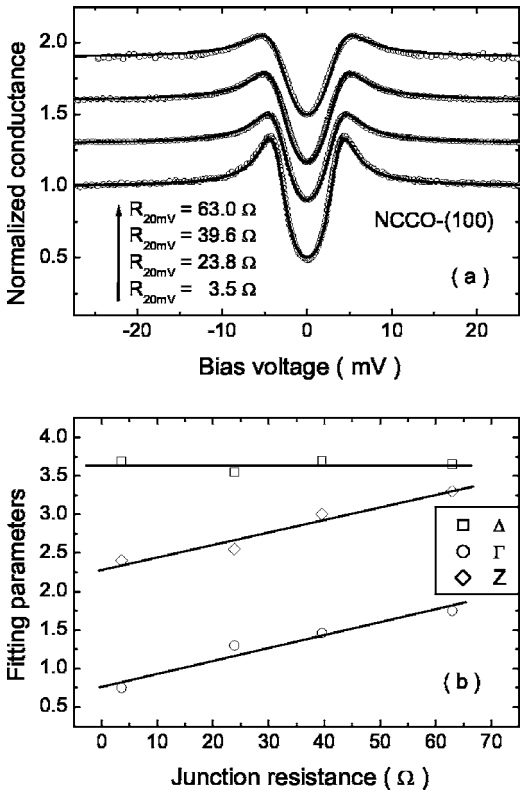

FIG. 8. (a) The normalized spectra measured at a fixed position on the sample surface with various junction resistance in a large resistive range. The open circles denote the experimental data and the solid lines indicate the fitting to the *s*-wave extended BTK model. (b) The fitting parameters for the spectra presented in (a).

both (110) and (100) directions are presented in Fig. 9, accompanied by the *s*-wave BTK fitting curves denoted by the solid lines. Because the spectra were affected by the critical current effect at higher temperature near T_c,[36] it is difficult to

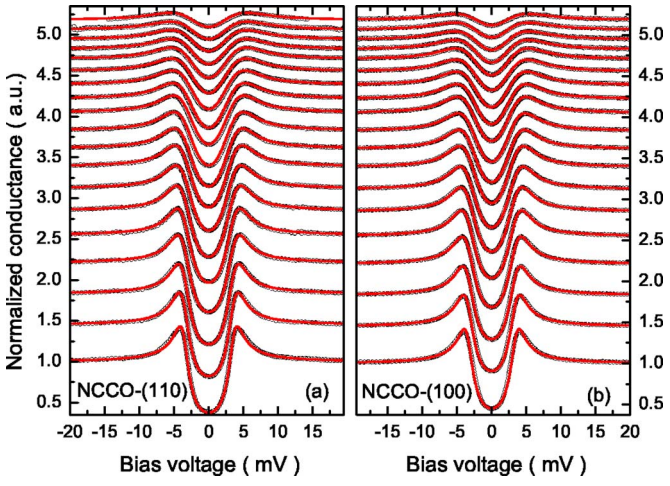

FIG. 9. (Color online) The temperature dependent normalized conductance and the *s*-wave BTK simulations for (a) (110) direction and (b) (100) direction. All the curves have been shifted upward except the lowest one for clarity. The temperature increases from 2 to 20 K with a interval of 1 K (from the bottom up). The theoretical simulations are denoted by solid lines.

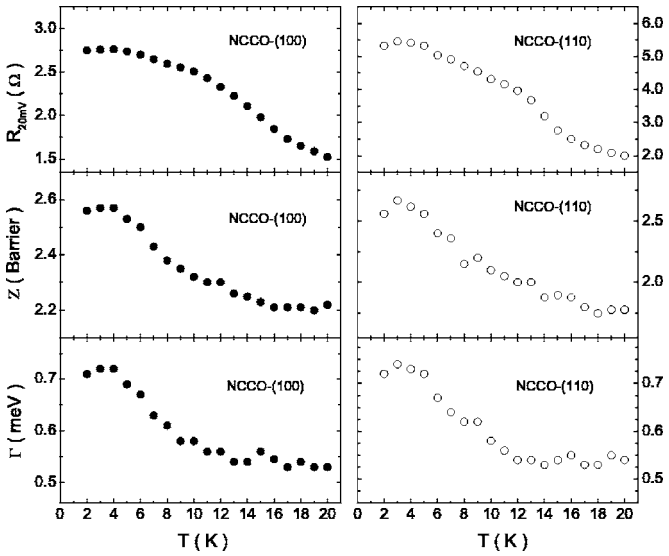

FIG. 10. The junction resistance measured at 20 mV, the best fitting parameters of the barrier height Z and the broadening parameter Γ corresponding to the simulations shown in Fig. 9. The junction resistances $R_{20\mathrm{mV}}$ of different spots on the sample surface possess the similar decay law with increasing temperature, indicating that the slight thermal expansion of the point-contact device. Correspondingly, the values of Z and Γ decrease with increasing temperature at first, then tend to be constant when the junction resistance becomes small enough because the minimal thickness of the barrier layer is achieved and the point flattening occurs.

determine the background for these temperatures. Therefore, these results have not been included in our theoretical analysis. All the parameters of the simulations shown in Fig. 9 are presented in Fig. 10 (the barrier height Z and the broadening parameter Γ) and Fig. 11 (superconducting energy gap Δ). The junction resistances measured at 20 mV ($R_{20\mathrm{mV}}$) are also given in Fig. 10.

The magnitude of $A=\Gamma/\Delta(0)<20\%$ presented is larger than that of the clean point-contact junction between normal metal and conventional superconductors which in general is smaller than 10%. However, considering the much shorter coherence length and faster exterior degradation of cuprates

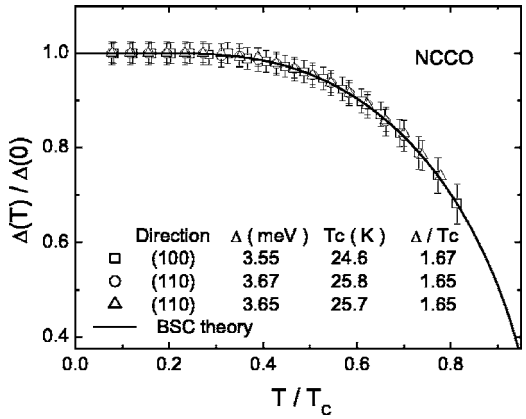

FIG. 11. The determined $\Delta(T)$ relations by fitting the temperature dependent tunneling spectra to the *s*-wave BTK theory. The solid line indicates the BCS prediction.

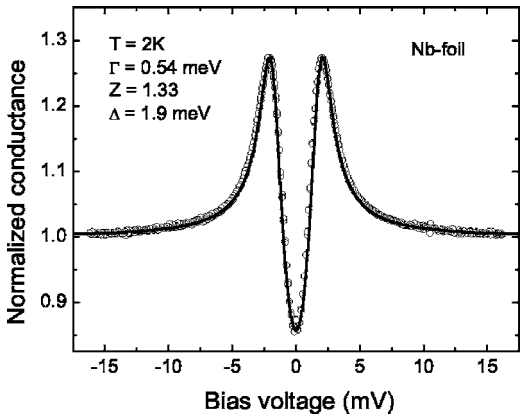

FIG. 12. The point contact spectrum measured at 2 K on the Nb foil exposed in air for a long time. The solid line denotes the *s*-wave BTK fitting. The obtained value of $A=\Gamma/\Delta(0)=0.28$ is much larger than that obtained from Au/NCCO tunneling in this work.

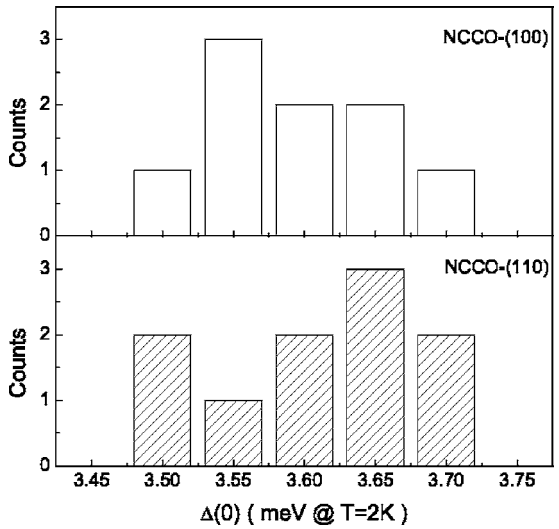

FIG. 13. Statistical chart of the $\Delta(0)$-values determined by the measurements at many different positions on the sample surfaces. The *y*-axis denotes the occurring times for a given gap-value specified by the *x*-axis.

than that of the conventional superconductors, one can easily understand the larger A. Actually, a large A ($>20\%$) is often obtained on the oxidized surface of Nb foil, a typical conventional superconductor, as shown in Fig. 12. The lowest value of $A=17\%$ achieved in this work is much smaller than the previous report of $A\approx 1$ by STM measurements on NCCO single crystal.[13]

As shown in Fig. 11, the normalized gap function $\Delta(T)$ determined by the fitting procedure can be well described by BCS theory, yielding a gap ratio $\Delta(0)/k_BT_c\approx 1.66$, which is very close to the theoretical value of 1.76. Such consistency between the tunneling data of cuprates and the theoretical model over a wide temperature range (between 0 K and T_c) is surprising. In order to determine the repeatability of such temperature-dependent measurements, we plot in Fig. 11 two $\Delta(T)$ relations obtained at two different positions for the (110) direction. All the $\Delta(T)$ functions obtained along both (110) and (100) directions and from different positions follow the BCS theory in a normalized scale. The T_c values derived from this figure are between 24.5–26 K, near the bulk transition temperature $T_c\approx 25.6$ K.

The distribution of the superconducting energy gap $\Delta(0)$ derived from the spectral measurements at many different positions are shown in Fig. 13. There is no obvious difference between the data obtained from (110) and (100) directions. The value of $\Delta(0)$ varies in a narrow range from 3.50 to 3.70, indicating the good homogeneity of the superconductivity in the investigated regions.

C. Tunneling spectra of $La_{1.89}Sr_{0.11}CuO_4$ (LSCO)

As a comparison, the directional tunneling spectra along both (100) and (110) directions were also studied on the LSCO single crystal, which has a typical $d_{x^2-y^2}$-wave pairing symmetry (as checked recently by specific heat).[37] The measured spectra at various temperatures are presented in Fig. 14. For the (100) direction at low temperatures, two clear coherence peaks appear in the spectra and no ZBCP can be observed. While for the (110)-oriented spectra, a prominent ZBCP was observed, accompanied by the disappearance of the coherence peaks. With the increasing temperature, all of these characteristics became weaker and weaker and eventually vanish around T_c. As mentioned above, photoemission experiments have proved that surface degradation resulting from air exposure form orders of magnitude faster on LSCO

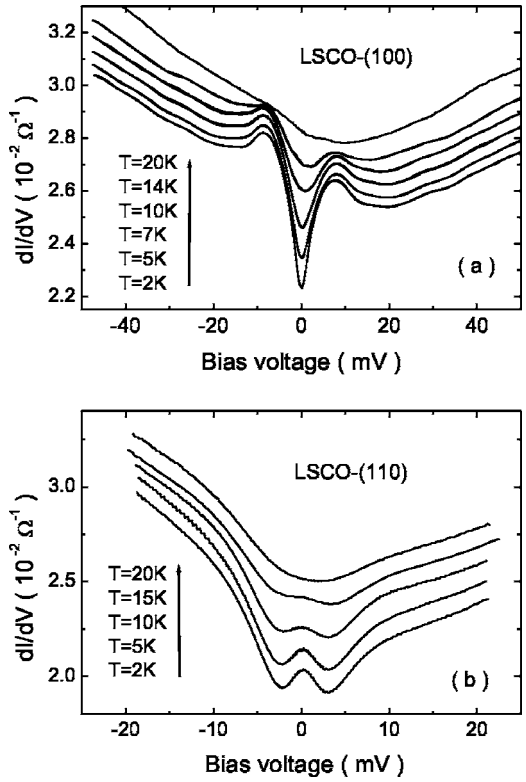

FIG. 14. Temperature dependent tunneling spectra of $La_{1.89}Sr_{0.11}CuO_4$ single crystal measured along (a) (100) direction and (b) (110) direction. The distinct spectral characteristics of these two directions are obviously different from the case of NCCO.

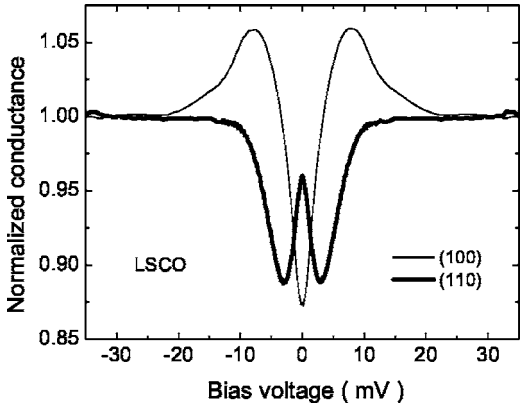

FIG. 15. Normalized tunneling spectra of $T=2$ K. Thick and thin solid lines indicate (110) and (100) directions, respectively. The remarkable difference between the cases along the two axes is in good agreement with the *d*-wave theory.

than NCCO, due to the existence of reactive alkaline earth elements in LSCO.[26] Therefore, the surface of LSCO degraded quickly before being put into the helium gas environment, which directly affected the subsequent spectral measurements. That is, the injecting quasiparticles felt the strong scattering effect from the surface barrier layer (resulting in a very large spectral broadening factor), i.e., the measured spectra were badly smeared. As shown in Fig. 14, the superconducting characteristics nearly completely disappear above 20 K, which is much lower than the bulk critical temperature $T_c \approx 28$ K.

In order to further demonstrate the spectral differences along the two directions, the spectra of $T=2$ K have been normalized using the higher bias backgrounds, as shown in Fig. 15. Although the strong scattering effect has severely smeared the spectra and made the quantitative analysis difficult, the coherence peaks around gap energy are depressed and a ZBCP appears when the tunneling direction changes from (100) to (110), as expected from the *d*-wave theory. These spectra are also consistent with the results obtained on the $La_{2-x}Sr_xCuO_4$/Ag junctions fabricated using a ramp-edge technique.[38]

D. Anisotropic *s*-wave and two-band models

In this section, we try to explain our experimental data with other possible models. In Ref. 13, the authors ascribed the unphysically large A ($A=\Gamma/\Delta \sim 1$) to the unreasonable assumption of isotropic *s*-wave symmetry. They found that if the maximum value of Γ/Δ was assumed to be 0.2, similar to YBCO, reasonable fitting is obtained by assuming anisotropic *s*-wave symmetry, namely, $\Delta(\theta)=\Delta_0+\Delta_1\cos(4\theta)$. Comparing this previous report with the present work, we find that the large value of A is mainly due to the surface degradation. Nonetheless, the anisotropic *s*-wave symmetry seems to be reasonable considering the crystallographic symmetry and the topology of Fermi surface (FS) of NCCO.[39,40] In Fig. 16(a), the best fitting to such anisotropic *s*-wave model is presented for both (110) and (100) directions. Recently, the ARPES experiment revealed another form of the gap function described as $\Delta(\theta)=\Delta_0\cdot|\cos(2\theta)-0.3\cos(6\theta)|$. Such $\Delta(\theta)$ function has also been tried in our fittings as shown in Fig. 16(b). All the parameters for the theoretical simulations of Fig. 16 are listed in Table II. It is found that the isotropic *s*-wave is the best candidate among the three *s*-wave models mentioned above.

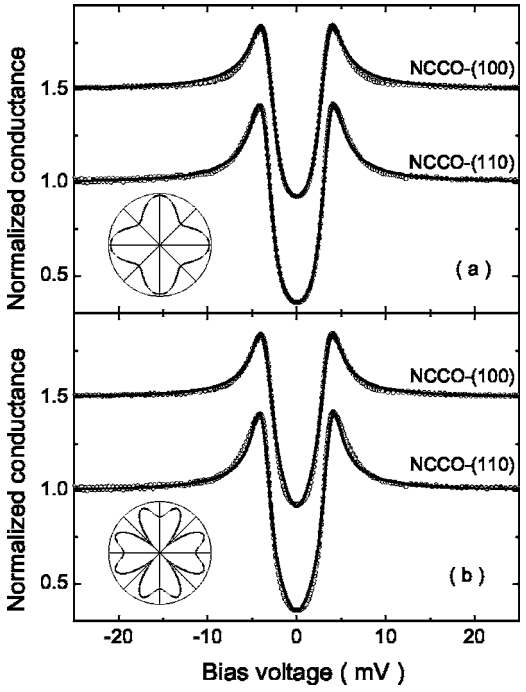

FIG. 16. Fitting the directional tunneling spectra to the anisotropic *s*-wave model with gap functions of (a) $\Delta(\theta)=\Delta_0+\Delta_1\cos(4\theta)$ and (b) $\Delta(\theta)=\Delta_0\cdot|\cos(2\theta)-0.3\cos(6\theta)|$. The insets are the schematic drawing of the angle-dependent energy gaps. The best fitting to the first type of anisotropic *s*-wave model has the value of Δ_1/Δ_0 smaller than 15% which is negligible within the fitting precision. If the second model is accepted, the simulations are also not bad as a whole, but cannot fit very well the spectral shape around zero bias.

Recent ARPES experiments[41,42] revealed the doping evolution of the Fermi surface (FS) in $Nd_{2-x}Ce_xCuO_4$. At low doping, a small Fermi pocket appears around $(\pi,0)$. Upon increasing doping, another pocket begins to form around $(\pi/2,\pi/2)$ and eventually at optimal doping $x=0.15$ several FS pieces evolve into a large curve around (π,π). These findings were effectively described as a two-band system.[40] Most recently, Luo *et al.*[43] used a weakly coupled two-band

TABLE II. The parameters for the fitting presented in Fig. 16.

Label	Δ_0 (meV)	Δ_1 (meV)	Z	Γ (meV)	Γ/Δ
(a) (110)	3.58	0.46	2.95	0.68	0.17
(a) (100)	3.45	0.44	2.80	0.84	0.21
(b) (110)	4.50	None	3.20	0.54	0.12
(b) (100)	4.30	None	3.10	0.64	0.15

BCS-like model to account for the low energy electromagnetic response of superconducting quasiparticles in electron-doped materials. The special angle dependence of the energy gap observed in Ref. 11 [as shown in the inset of Fig. 16(b)] may be a reflection of the two-band model. In the analysis in Ref. 43, both the pairing symmetries of band 1 and band 2 are assumed to be of the $d_{x^2-y^2}$ type in order to achieve the best fitting for the superfluid density data, in which the labels 1 and 2 represent the bands contributing to the FS centered at $(\pm\pi,0)$, $(0,\pm\pi)$, and $(\pm\pi/2,\pm\pi/2)$, respectively. However, as pointed out by the authors, there is a finite excitation gap in band 1 since the nodal lines do not intersect with the FS of that band if the system is not heavily overdoped. This indicates that the superconducting state of NCCO is actually a mixture of *d*- and *s*-wave pairing states. In other words, this analysis cannot definitely determine whether the pairing symmetry of band 1 is *s*- or *d*-wave type. Based on this two-band model, we calculated the directional tunneling spectra by assuming different pairing symmetries (*s*- or *d*-wave) for band 1 while definite $d_{x^2-y^2}$ for band 2. In these calculations, the ratio of the contribution from band 1 to that from band 2 was chosen according to the discussions in Ref. 43. If only the *d*-wave symmetry of band 1 is accepted, a prominent ZBCP will appear in the spectra along the (110) direction. That is, the *s*-wave symmetry of band 1 is required in the fitting procedure. Moreover, the best fit needs a much larger value of $A=\Gamma/\Delta$ for band 2 than that for band 1 as shown in Fig. 17. This is possibly due in part to the strong depression of the *d*-wave superconductivity on the sample surface while the essential origin is yet to be found. Such a mixture of superconductivity coming from two bands may be another possible reason of the contradicting reports on the pairing symmetry by different experiments. For example, the phase-sensitive measurements[6,7] may selectively detect the gap information from band 2 which crosses the Fermi surface near $(\pi/2,\pi/2)$. In addition, such interband mixture may also be responsible to the doping dependent pairing symmetry observed in $Pr_{2-x}Ce_xCuO_4$ thin films.[19] In any case, the *s*-wave pairing symmetry appears to be an important component in the superconductivity of optimally-doped NCCO.

In summary, the directional tunneling spectra along the (110) and (100) axes on the NCCO and LSCO single crystals illustrate clearly distinct pairing symmetries. In contrast to the results of LSCO ($x=0.11$), no ZBCP was observed for NCCO ($x=0.15$) along the two different directions while sharp coherence peaks are existent for both directions, which disagrees with the pure *d*-wave pairing symmetry. The almost identical spectral shapes for the two directions on NCCO can be understood in the framework of *s*-wave BTK theory, leading to a BCS type temperature dependence of energy gap with the ratio of $\Delta/k_BT_c\approx 1.66$. The present work provides evidence for the *s*-wave component in the superconductivity of the optimally-doped NCCO, which should mainly come from the band crossing the FS around $(\pm\pi,0)$ and $(0,\pm\pi)$ if a two-band model is accepted.

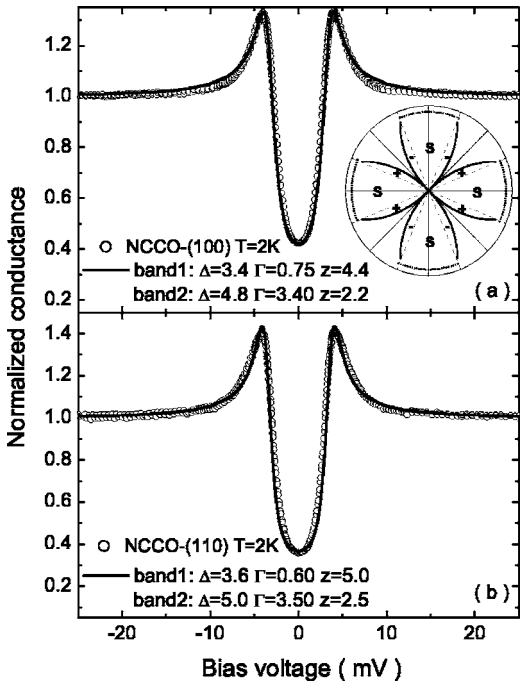

FIG. 17. Fitting the directional tunneling spectra to the two-band model: (a) along (100) direction and (b) along (110) direction. All the fitting parameters are listed in the corresponding panels. The angle-dependent gap amplitude and sign are described in the inset. Dotted lines indicate the *s*-wave component while the solid lines indicate the *d*-wave component.

ACKNOWLEDGMENTS

The authors thank Professor T. Xiang and Dr. H. G. Luo for fruitful discussions. The work is supported by the National Science Foundation of China, the Ministry of Science and Technology of China, and the Chinese Academy of Sciences with the Knowledge Innovation Project. Pengcheng Dai is supported by the U. S. NSF DMR-0139882, DOE No. DE-AC05-00OR22725 with UT/Battelle, LLC., and by NSF of China under Contract No. 10128408. We thank Dr. Y. G. Shi for the provision of some chemicals.

*Email address: shanlei@ssc.iphy.ac.cn

†Email address: hhwen@aphy.iphy.ac.cn

[1] J. Orenstein and A. J. Millis, Science **288**, 468 (2000).

[2] Y. Tokura, H. Takagi, and S. Uchida, Nature (London) **337**, 345 (1989).

[3] For a review, see for example, C. C. Tsuei and J. R. Kirtley, Rev. Mod. Phys. **72**, 969 (2000), and references therein.

[4] N. P. Armitage, D. H. Lu, D. L. Feng, C. Kim, A. Damascelli, K. M. Shen, F. Ronning, Z.-X. Shen, Y. Onose, Y. Taguchi, and Y. Tokura, Phys. Rev. Lett. **86**, 1126 (2001); T. Sato, T. Kamiyama, T. Takahashi, K. Kurahashi, and K. Yamada, Science **291**, 1517 (2001).

[5] Hamza Balci, V. N. Smolyaninova, P. Fournier, Amlan Biswas, and R. L. Greene, Phys. Rev. B **66**, 174510 (2002).
[6] C. C. Tsuei and J. R. Kirtley, Phys. Rev. Lett. **85**, 182 (2000).
[7] B. Chesca, M. Seifried, T. Dahm, N. Sachopohl, D. Koelle, R. Kleiner, and A. Tsukada, Phys. Rev. B **71**, 104504 (2005).
[8] J. D. Kokales, Patrick Fournier, Lucia V. Mercaldo, Vladimir V. Talanov, Richard L. Greene, and Steven M. Anlage, Phys. Rev. Lett. **85**, 3696 (2000); R. Prozorov, R. W. Giannetta, P. Fournier, and R. L. Greene, Phys. Rev. Lett. **85**, 3700 (2000).
[9] A. Snezhko, R. Prozorov, D. D. Lawrie, R. W. Giannetta, J. Gauthier, J. Renaud, and P. Fournier, Phys. Rev. Lett. **92**, 157005 (2004).
[10] G. Blumberg, A. Koitzsch, A. Gozar, B. S. Dennis, C. A. Kendziora, P. Fournier, and R. L. Greene, Phys. Rev. Lett. **88**, 107002 (2002).
[11] H. Matsui, K. Terashima, T. Sato, T. Takahashi, M. Fujita, and K. Yamada, Phys. Rev. Lett. **95**, 017003 (2005).
[12] C.-T. Chen, P. Seneor, N.-C. Yeh, R. P. Vasquez, L. D. Bell, C. U. Jung, J. Y. Kim, Min-Seok Park, Heon-Jung Kim, and Sung-Ik Lee, Phys. Rev. Lett. **88**, 227002 (2002).
[13] S. Kashiwaya, T. Ito, K. Oka, S. Ueno, H. Takashima, M. Koyanagi, Y. Tanaka, and K. Kajimura, Phys. Rev. B **57**, 8680 (1998).
[14] Z. Y. Liu, H. H. Wen, L. Shan, H. P. Yang, X. F. Lu, H. Gao, C. U. Jung, J. Y. Kim, Min-Seok Park, Heon-Jung Kim, and Sung-Ik Lee, Europhys. Lett. **69**, 263 (2005).
[15] L. Alff, S. Meyer, S. Kleefisch, U. Schoop, A. Marx, H. Sato, M. Naito, and R. Gross, Phys. Rev. Lett. **83**, 2644 (1999).
[16] John A. Skinta, Thomas R. Lemberger, T. Greibe, and M. Naito, Phys. Rev. Lett. **88**, 207003 (2002).
[17] M.-S. Kim, J. A. Skinta, T. R. Lemberger, A. Tsukada, and M. Naito, Phys. Rev. Lett. **91**, 087001 (2003).
[18] J. A. Skinta, M.-S. Kim, T. R. Lemberger, T. Greibe, and M. Naito, Phys. Rev. Lett. **88**, 207005 (2002).
[19] A. Biswas, P. Fournier, M. M. Qazilbash, V. N. Smolyaninova, Hamza Balci, and R. L. Greene, Phys. Rev. Lett. **88**, 207004 (2002).
[20] H. Balci and R. L. Greene, Phys. Rev. Lett. **93**, 067001 (2004).
[21] Y. Onose, Y. Taguchi, K. Ishizaka, and Y. Tokura, Phys. Rev. Lett. **87**, 217001 (2001).
[22] F. Zhou, W. X. Ti, J. W. Xiong, Z. X. Zhao, X. L. Dong, P. H. Hor, Z. H. Zhang, and W. K. Chu, Supercond. Sci. Technol. **16**, L7 (2003).
[23] L. Shan, H. J. Tao, H. Gao, Z. Z. Li, Z. A. Ren, G. C. Che, and H. H. Wen, Phys. Rev. B **68**, 144510 (2003).
[24] R. P. Vasquez, B. D. Hunt, and M. C. Foote, Appl. Phys. Lett. **53**, 2692 (1988).
[25] Shao-Xiong Li, Hong-Jie Tao, Yi Xuan, Bo-Ru Zhao, and Zhong-Xian Zhao, Appl. Phys. Lett. **76**, 3466 (2000).
[26] R. P. Vasquez, J. Electron Spectrosc. Relat. Phenom. **66**, 209 (1994).
[27] G. E. Blonder, M. Tinkham, and T. M. Klapwijk, Phys. Rev. B **25**, 4515 (1982).
[28] G. E. Blonder and M. Tinkham, Phys. Rev. B **27**, 112 (1982).
[29] S. Kashiwaya, N. Matsubara, B. Prijamboedi, H. Shibata, K. Takita, H. Kashiwaya, Y. Asano, and Y. Tanaka, J. Low Temp. Phys. **131**, 327 (2003).
[30] A. Mourachkine, Europhys. Lett. **50**, 663 (2000).
[31] Chia-Ren Hu, Phys. Rev. Lett. **72**, 1526 (1994).
[32] Y. Tanaka and S. Kashiwaya, Phys. Rev. Lett. **74**, 3451 (1995); Phys. Rev. B **53**, 9371 (1996).
[33] S. Kashiwaya and Y. Tanaka, Rep. Prog. Phys. **63**, 1641 (2000).
[34] R. C. Dynes, J. P. Garno, G. B. Hertel, and T. P. Orlando, Phys. Rev. Lett. **53**, 2437 (1984).
[35] A. Plecenník, M. Grajcar, S. Benacka, P. Seidel, and A. Pfuch, Phys. Rev. B **49**, 10016 (1994).
[36] G. Sheet, S. Mukhopadhyay, and P. Raychaudhuri, Phys. Rev. B **69**, 134507 (2004).
[37] H. H. Wen, Z. Y. Liu, F. Zhou, J. W. Xiong, W. X. Ti, T. Xiang, S. Komiya, X. F. Sun, and Y. Ando, Phys. Rev. B **70**, 214505 (2004).
[38] T. Miyake, T. Imaizumi, and I. Iguchi, Phys. Rev. B **68**, 214520 (2003).
[39] D. M. King, Z. X. Shen, D. S. Dessau, B. O. Wells, W. E. Spicer, A. J. Arko, D. S. Marshall, J. DiCarlo, A. G. Loeser, C. H. Park, E. R. Ratner, J. L. Peng, Z. Y. Li, and R. L. Greene, Phys. Rev. Lett. **70**, 3159 (1993).
[40] Qingshan Yuan, Yan Chen, T. K. Lee, and C. S. Ting, Phys. Rev. B **69**, 214523 (2004).
[41] N. P. Armitage, F. Ronning, D. H. Lu, C. Kim, A. Damascelli, K. M. Shen, D. L. Feng, H. Eisaki, Z. X. Shen, P. K. Mang, N. Kaneko, M. Greven, Y. Onose, Y. Taguchi, and Y. Tokura, Phys. Rev. Lett. **88**, 257001 (2002).
[42] A. Damacelli, Z. Hussain, and Z. X. Shen, Rev. Mod. Phys. **75**, 473 (2003).
[43] H. G. Luo and T. Xiang, Phys. Rev. Lett. **94**, 027001 (2005).